Nanostructure design of amorphous $FePO_4$ facilitated by a virus for 3 V lithium ion battery cathodes†

Yun Jung Lee[a] and Angela M. Belcher*[ab]

Received 5th August 2010, Accepted 23rd September 2010
DOI: 10.1039/c0jm02544e

Amorphous iron phosphate nanowires with diameters of 10 to 20 nm were synthesized using genetically engineered M13 virus for lithium ion battery cathodes. Hydrolysis of Fe^{3+} ions has been effectively suppressed by forming conjugates with the virus and synthesizing at low temperature, 4 °C. The M13 virus biological template facilitated elaborate nanostructure design and environmentally benign, low temperature synthesis. By implementing heterostructures with silver, we demonstrated experimentally that uniformly distributed Ag nanoparticles throughout the whole structure appeared more advantageous than locally limited network formation by Ag nanowires in enhancing overall electronic conductivity of the entire system, thereby improving battery performances. Electrochemical properties were further improved by dehydration of structural waters. The synergetic use of biological template and synthetic chemistry could enable the synthesis of anhydrous a-$FePO_4$ without thermal treatment *via* low-temperature and eco-efficient chemistry. The first discharge capacity at a discharge rate of *C*/10 and 1*C* was 165 mA h g^{-1} (93% of the theoretical value) and 110 mA h g^{-1}, respectively. These electrochemical properties are comparable to the best reported values for a-$FePO_4$ synthesized at high temperature. In this study, we set the important step for the practical applications of biological approaches in designing and fabricating energy devices, which may be a promising alternative to the traditional processing techniques that consume energy and are costly.

Introduction

Although the lithium ion battery has a high energy density, it has been considered as a low-power device (slow charge/discharge). However, recent advances in lithium rechargeable battery technology enabled both high energy density (~200 Wh kg^{-1}) and high power density (~4.5 kW kg^{-1}) for the application to hybrid and electric cars.[1] Since the energy storage mechanism of lithium ion batteries depends on the movement of Li^+ ions and electrons through the electrode materials, increasing transport of Li^+ ions and electrons in electrodes can enhance energy storage at high charge and discharge rates. In other words, sluggish Li^+ ion/electron transport is one of the main reasons for kinetic limitations. Reducing dimensions of the electrode materials to the nanometre regime have proven to be effective in expediting both electrons and ions movement. Use of smaller particles not only reduces the traveling path for electrons and ions but also increases the interfaces between the particle and electrolyte facilitating Li^+ ion exchange across the interfaces. Carbon layer surface painting[2] and conducting additives[3,4] have been the other main strategies to address the kinetic constraints. Despite several disadvantages such as low packing densities and high risk of side reactions associated with large surface area, controlling nanostructures[5–7] already have shown their impact on activating such class of materials as transition metal phosphate cathode materials.[7–9] This phosphate family was initially not considered as potential electrode materials due to the aforementioned kinetic limitations such as low electronic and ionic conductivities. Among them, iron phosphate based materials have assumed paramount importance as promising Li ion battery positive electrode materials due to the abundance of iron, low toxicity and enhanced safety especially for high power applications.[10] The kinetic limitations have been relieved mainly by nanosizing[11] and carbon nanopainting.[2] While crystalline $LiFePO_4$ is being intensively explored, little attention has been paid to $FePO_4$ since Li-containing positive electrodes are required to be paired with the most common negative electrode carbon for current lithium rechargeable battery system. Although this material is not compatible with the available battery configuration for now, the use of Li-free positive electrode could urge the implementation of Li-containing negative electrode such as Li-metal alloys and Li-metal nitrides. In previous work, amorphous $FePO_4$ showed reversible lithium intercalation at about 3 V and unlike crystalline $LiFePO_4$, the potential profile showed single phase reaction.[12,13] Hydrated amorphous iron phosphates (a-$FePO_4 \cdot nH_2O$, n = 0–4) crystallize to α-quartz structure (trigonal $FePO_4$) in which Fe^{3+} ions are tetrahedrally coordinated by oxygen.[14,15] The best performance of iron phosphate as cathodes was reported by adopting mesoporous structures with residual surface carbon coatings. This mesoporous iron phosphate could deliver 110 mA h g^{-1} at 1*C* and 85 mA h g^{-1} at 3*C* rate.[16] However, the fabrication of nanosized particles for better performance is still challenging since the materials require at least 350 °C for

[a]*Department of Materials Science and Engineering, Massachusetts Institute of Technology, Cambridge, Massachusetts, 02139, USA. E-mail: belcher@mit.edu*
[b]*Department of Biological Engineering, Massachusetts Institute of Technology, Cambridge, Massachusetts, 02139, USA*

† Electronic supplementary information (ESI) available: TEM images of $FePO_4 \cdot H_2O$ powder without virus, a-$FePO_4 \cdot H_2O$/Ag nanowires, and (Ag)a-$FePO_4 \cdot H_2O$. TGA curve of AgCl. Impedance impedance response of a-$FePO_4 \cdot H_2O$, a-$FePO_4 \cdot H_2O$/Ag NW and (Ag)a-$FePO_4$ viral nanowires. See DOI: 10.1039/c0jm02544e

structure formation and carbon coating. In addition to this functional perspective, environmental and energy saving considerations require low temperature and environmentally sustainable ways for making energy devices. These considerations motivated us to use biological systems for the growth and assembly of materials for the energy system. Biological systems feature the exquisitely self-organized hierarchical structures as well as the unique capabilities for environmentally benign materials synthesis. The filamentous M13 virus has a high aspect ratio with, approximately, a 6.5 nm diameter and an 880 nm length. There are ~2700 identical protein subunits of genetically modifiable α-helix on the major coat protein.[17] The safety of M13 virus was recently shown in human medical trials as tumor-targeting vehicles. The virus was non-toxic, had no adverse allergic response, and elicited submaximal humoral immune response.[18] The M13 virus-based toolkit has served as unique templates for the growth and assembly of various functional materials through genetically programmable ways.[19–21] Our group reported successful nanowire synthesis of materials such as Co_3O_4,[21] amorphous $FePO_4$[7] for the application to lithium ion batteries. Its unique characteristics of high aspect ratio, surface functionality and material specific binding have been applied to lithium ion battery electrodes fabrication[7,21,22] and considered as an elegant way for addressing challenges that lithium ion battery technologies are concerned for.[1] Here we present more extensive studies on the M13 virus-enabled low temperature synthesis and nanostructure architecting of amorphous iron phosphate (a-$FePO_4 \cdot nH_2O$, $n = 0$ or 1) materials for lithium ion battery cathodes. By comparing battery performance of various structures incorporating silver, this work showed the importance of designing material structures at the nanoscale aided by bio-assembly.

Experimental

Synthesis of virus-based electrode

The viruses were amplified using *Escherichia coli* bacterial medium and purified by standard PEG/NaCl precipitation method. (i) For the a-$FePO_4 \cdot H_2O$ synthesis, 200 μl aqueous virus solution (2×10^{11} PFU ml^{-1}) were first incubated with 1 mM, 1 ml $FeCl_3 \cdot 6H_2O$ for 24 hours at 4 °C. After reacting with 1 mM, 1 ml Na_3PO_4 at pH = 7.5 for 24 hours at 4 °C, the growth was completed. The final solution was filtered and washed with water several times. The collected powder was dried in a 100 °C vacuum oven overnight. (ii) For a-$FePO_4 \cdot H_2O$/Ag nanowire mixture synthesis, Ag nanowires were synthesized on the separate viral template. First, 50 μl phage solution in 0.1 M TBS buffer (2×10^{11} PFU ml^{-1}) were dialyzed against pH = 9.5 water overnight, followed by incubation with 2 mM, 1 ml silver acetate ($AgOOCCH_3$) solution for 12 hours in the dark at 37 °C. All solutions were aqueous after the dialysis. The Ag ions were reduced by 1 ml of 10 mM sodium borohydride ($NaBH_4$) at room temperature. The resulting Ag viral nanowires were dialyzed against pure water (Millipore Milli-Q, 18.2 MΩ cm) overnight. The dialyzed solution of Ag viral nanowires was added to the $FePO_4 \cdot H_2O$ solution prepared following (i). (iii) For the (Ag)a-$FePO_4 \cdot H_2O$ synthesis, 1 ml virus solution in 0.1 M TBS buffer (2×10^{11} PFU ml^{-1}) was dialyzed against pH = 9.5 water overnight, followed by incubation with 1 mM, 1 ml silver acetate ($AgOOCCH_3$) solution for 12 hours in the dark at room temperature. All solutions were aqueous after the virus dialysis. The Ag nanoparticles (NPs) were formed by reducing with 5 mM, 1 ml sodium borohydride ($NaBH_4$) for 4 hours at room temperature. This Ag NPs-loaded virus solution was dialyzed against pure water at room temperature to remove remaining ions. (Ag)a-$FePO_4 \cdot H_2O$ viral nanowires were synthesized on these Ag NPs-loaded virus using $Fe(NO_3)_3 \cdot 9H_2O$ precursor. The Ag NPs-loaded viruses were incubated with 1.33 mM, 9 ml $Fe(NO_3)_3 \cdot 9H_2O$ to have final concentration of 1 mM for 24 hours at 4 °C in order to suppress hydrolysis of Fe^{3+} ions into oxide/hydroxide. Amorphous $FePO_4 \cdot H_2O$ nanowires were produced after reacting with 1 mM, 12 ml Na_3PO_4 at pH = 7.5 for 24 hours at 4 °C. The final solution was filtered and washed with water several times. The collected powder was dried in a 100 °C vacuum oven overnight. (iv) For the (AgCl)a-$FePO_4$ synthesis, the procedure was the same for the growth of (Ag)a-$FePO_4 \cdot H_2O$ nanowires, but $FeCl_3 \cdot 6H_2O$ precursor was used instead of $Fe(NO_3)_3 \cdot 9H_2O$.

Structural and chemical characterizations

The microstructure of nanowires was analyzed with Transmission Electron Microscopy (JEOL 200CX TEM). For TEM analysis, solutions were dropped on copper grids, washed with distilled water several times and dried. Chemical composition was determined by DCP-AES (Luvak, Boylston, MA). For ThermoGravimetric Analysis (TGA), a RGA Q50 (TA instrument) apparatus was used. Samples placed on a platinum pan were preheated to 100 °C and held for 5 min to remove surface absorbed water. After cooling down to 30 °C, samples were heated to 700 °C at a heating rate of 10 °C min^{-1} in 90 ml min^{-1} nitrogen flow and 10 ml min^{-1} helium flow. X-Ray Diffraction (XRD) was done using Cu Kα radiation and a Rigaku RU300 powder diffractometer.

Electrochemical characterization

For positive electrode preparation, viral a-$FePO_4$ nanowires were mixed with Super P® (TIMCAL, Super P® Li) carbon black and polytetrafluoroethylene (PTFE) binder. (A) For mixing ratio of powder tested : Super P® carbon : PTFE = 80 : 15 : 5. Detailed mass ratios of each component in electrodes are: (i) for a-$FePO_4 \cdot H_2O$, a-$FePO_4 \cdot H_2O$: virus: Super P® carbon : PTFE = 66.6 : 13.4 : 15 : 5. (ii) For Ag nanowire mixed a-$FePO_4 \cdot H_2O$, a-$FePO_4 \cdot H_2O$: virus : Ag : Super P® carbon : PTFE = 63.3 : 12.7 : 4 : 15 : 5. (iii) For (Ag)a-$FePO_4 \cdot H_2O$, a-$FePO_4 \cdot H_2O$: virus : Ag : Super P® carbon : PTFE = 67.6 : 8.3 : 4.1 : 15 : 5. (iv) For (AgCl)a-$FePO_4$, a-$FePO_4$: virus : AgCl : Super P® carbon : PTFE = 61.3 : 14.5 : 4.2 : 15 : 5. (B) For mixing ratio of powder tested : Super P® carbon : PTFE = 70 : 25 : 5. Detailed mass ratio of each component in electrodes are: (i) for a-$FePO_4 \cdot H_2O$, a-$FePO_4 \cdot H_2O$: virus : Super P® carbon : PTFE = 58.3 : 11.7 : 25 : 5. (ii) For (Ag)a-$FePO_4 \cdot H_2O$, a-$FePO_4 \cdot H_2O$: virus : Ag : Super P® carbon : PTFE = 59.1 : 7.3 : 3 : 3.6 : 25 : 5. (iii) For (AgCl)a-$FePO_4$, a-$FePO_4$: virus : AgCl : Super P® carbon : PTFE = 52.9 : 13.4 : 3.7 : 25 : 5. The mixture was roll milled and punched

into disks with diameters of 8 mm. The typical electrode thickness was 20 to 40 μm. The cell was assembled in an argon filled glove box using lithium foil as a negative electrode, a microporous polymer separator (Celgard 3501™) and liquid electrolyte mixtures of 1 M $LiPF_6$ in ethylene carbonate : dimethyl carbonate (EC : DMC) = 1 : 1 in volume ratio (Ferro Corporation). The testing cell was a coin cell configuration. The assembled cell was galvanostatically tested using a Solatron Analytical 1470E potentiostat. Rates are reported in *C*-rate convention, where *C*/*n* is the rate (current per gram) corresponding to complete charging or discharging to the theoretical capacity of the materials in *n* hours. Here, 1*C* corresponds to 178 mA g^{-1} for (AgCl)a-$FePO_4$ and 159 mA g^{-1} for a-$FePO_4 \cdot H_2O$ and (Ag)a-$FePO_4 \cdot H_2O$. At each rate, the test cell was fully charged before starting the first discharge by charging at *C*/10 rate to 4.3 V and applying constant voltage at 4.3 V until the current density was lower than *C*/100. Impedance measurements of the testing cell before and after galvanostatic test were done using Princeton Applied Research PARSTAT® 2273 potentiostat and impedance analyzer. The impedance response was obtained by applying 10 mV ac potential excitation in a frequency range from 10^5 to 0.1 Hz.

Results and discussion

Virus-enabled nanostructured cathode materials were first demonstrated by templating amorphous iron phosphate (a-$FePO_4 \cdot nH_2O$) on the E3/E4 virus. The clone we used was initially named E4. E4 is a modified M13 virus that has tetraglutamate (EEEE-) fused to the amino terminus of each copy of pVIII major coat protein. However, upon repeated rounds of amplification and followed by sequencing, the population of virus was determined to consist of mixture of three glutamate and four glutamate residues, so it is termed E3/E4. Due to the presence of extra carboxylic acid groups compared with wild-type M13 virus (M13KE), the E3/E4 virus exhibits increased ionic interactions with cations, and can serve as an efficient template for materials growth.[21–23]

Initial trials for the synthesis of virus enabled amorphous iron phosphates at room temperature were not successful. The loading of Fe^{3+} ions into the carboxylic acid containing polymer film was reported to be not very fast,[24] hence prolonged incubation of Fe^{3+} with E3/E4 virus was required to make uniform carboxylic group–Fe^{3+} ion conjugates along the E3/E4 virus. However, Fe^{3+} ions are easily hydrolyzed in aqueous conditions resulting in a yellowish solution of iron oxide/hydroxide. A short incubation time of 1 or 2 hours could prevent hydrolysis, however, the reaction products were not continuous nanowires along the virus but free particle aggregates formed non-specifically in the bulk of solution. In order to make uniform nanowires along the virus, incubation of Fe^{3+} ions with E3/E4 virus was done at 4 °C to suppress hydrolysis of Fe^{3+} ions during the synthesis process. To test the feasibility of 4 °C low temperature process for the stable E3/E4 virus–Fe^{3+} ion conjugate formation without hydrolysis, a solution containing Fe^{3+} ions was stored at 4 °C for 8 days. The solution containing Fe^{3+} ions stored in the presence of E3/E4 virus did not show a color change while the same solution without virus showed obvious color change to yellow after 8 days. In Fig. 1(a), E3/E4 viruses were imaged as

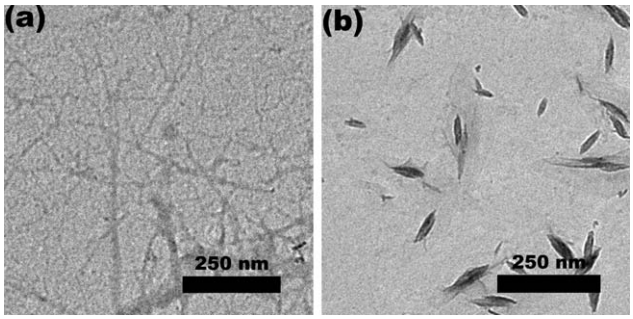

Fig. 1 Changes in Fe^{3+} ions stored at 4 °C for 8 days. TEM images of solutions containing Fe^{3+} ions. (a) With virus. Virus looked stained with Fe^{3+} ions indicating formation of E3/E4 virus–Fe^{3+} ion conjugates. (b) Without virus. Without virus, Fe^{3+} ions were hydrolyzed to needle-like crystals.

stained with Fe^{3+} ions indicating formation of E3/E4 virus–Fe^{3+} ion conjugates. In the solution without virus, needle-like crystals of iron oxide/hydroxide were formed in Fig. 1(b). There were no needle-like crystals in the solution containing E3/E4 virus. Therefore we speculate that Fe^{3+} ion–E3/E4 virus conjugates formation could suppress Fe^{3+} ions hydrolysis at 4 °C.

Process optimization resulted in 24 hours of Fe^{3+} ions incubation with E3/E4 virus and 24 hours of growth after the addition of Na_3PO_4 at 4 °C for the growth of amorphous iron phosphate (a-$FePO_4 \cdot nH_2O$) viral nanowires. X-Ray powder diffraction (XRD) was featureless confirming amorphous nature of $FePO_4$.[7] For structural analysis, transmission electron microscope (TEM) analysis was done. Fig. 2(a) shows TEM images of a-$FePO_4 \cdot nH_2O$ nanowires with particle sizes of 10 to 20 nm in diameter templated on the virus. In TEM-EDX analysis for the same nanowires (Fig. 2(b)), the presence of element Fe, P and O was clearly identified. The chemical analysis by direct current plasma atomic emission spectroscopy (DCP-AES)

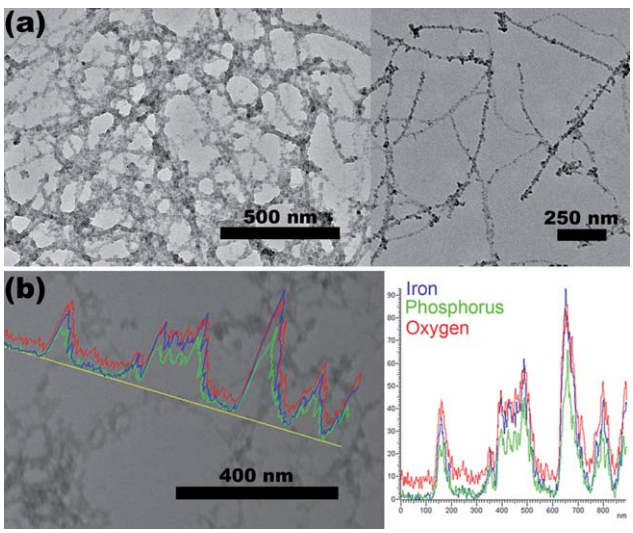

Fig. 2 a-$FePO_4 \cdot H_2O$ nanowires templated on the virus. (a) TEM images of a-$FePO_4 \cdot H_2O$ nanowires on E3/E4 virus. Particle size was 10–20 nm. (b) EDX showing the presence of Fe, P and O elements in the template nanowires.

confirmed the atomic ratio of Fe to P as 1 : 1. The contribution to the phosphorus contents from the DNA of virus itself (7270 phosphate group per one virus) is below 1%, and thus considered negligible. To determine structural water content in the synthesized nanowires, thermogravimetric analysis (TGA) was performed. Generally, hydrated a-$FePO_4$ (a-$FePO_4 \cdot nH_2O$, $n = 2$–4) is precipitated in aqueous solutions containing Fe^{3+} and PO_4^{3-} ions around neutral pH and anhydrous structures can be obtained through the dehydration of a-$FePO_4 \cdot nH_2O$ by thermal annealing at 400 °C. Most structural water in a-$FePO_4 \cdot nH_2O$ is removed from the structure around 200 °C.[12] Fig. 3(a) is a TGA curve of bare virus. Virus mainly decomposes between 200 and 500 °C and 13 wt% remains as residues. Based on this TGA curve of virus alone and the TGA curve from the synthesized viral amorphous iron phosphates, the structural water content was determined as 10.1 wt%, which corresponds to $n = 1$ in a-$FePO_4 \cdot nH_2O$. Therefore, the nanowires described above were denoted a-$FePO_4 \cdot H_2O$. Since we dried our viral powder at 100 °C in an oven under vacuum, structural water content was reduced to 1 molecule. Virus content was determined as 16.7 wt%.

Before testing viral a-$FePO_4 \cdot H_2O$ as a lithium ion battery cathode, electrochemical response of bare virus in the voltage window of interests was evaluated first. In Fig. 4, there was virtually no capacity observed at a rate of 15 mA g^{-1} (current corresponds to ~*C*/10 rate for a-$FePO_4 \cdot H_2O$ electrodes). At a very slow rate of 1.5 mA g^{-1} (current corresponds to ~*C*/100 rate for a-$FePO_4 \cdot H_2O$ electrodes), signs of irreversible oxidation were observed when the potential is over 4 V. Thus, we concluded

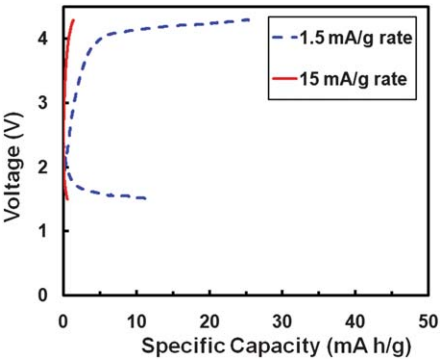

Fig. 4 Electrochemical response of the bare virus tested between 1.5 and 4.3 V. Electrodes were prepared with mass ratio of powder tested (bare virus) : Super P® carbon : PTFE = 70 : 25 : 5.

that the virus is electrochemically inactive under most testing conditions used in this study.

Electrochemical performance of viral a-$FePO_4 \cdot H_2O$ as lithium ion battery cathodes was evaluated (Fig. 5). In the first discharge profiles of Fig. 5(a), specific capacity at a rate of *C*/10 was 100 mA h g^{-1}, but the rate capability was not very good as shown in Fig. 5a and b. In Fig. 5(b), there is a capacity loss at the 2nd cycle, but capacity retention was stable after 2nd cycle. Capacity loss at the 2nd cycle is a characteristic of this a-$FePO_4 \cdot nH_2O$ material.[12,13,25] The a-$FePO_4 \cdot H_2O$ nanowires templated on the virus present slightly improved specific capacity compared to a-$FePO_4 \cdot H_2O$ powder sample synthesized by the same procedure without virus, due to the nanosized particles formation on the

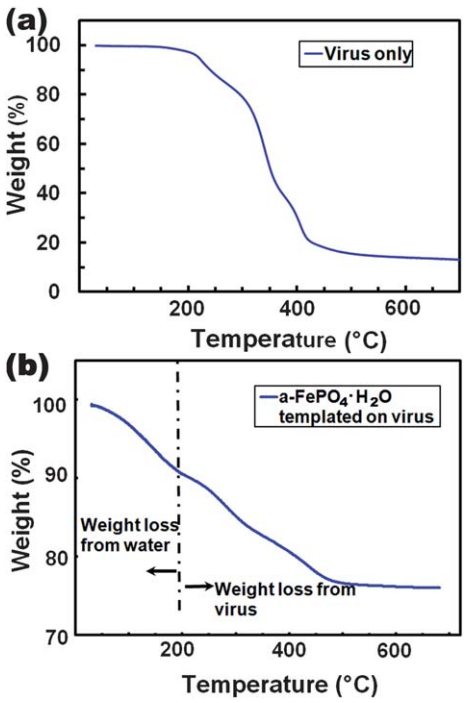

Fig. 3 ThermoGravimetric Analysis (TGA) curves of (a) virus only. Virus mainly decomposes at temperature range 200–500 °C and 13 wt% remains as residues. (b) a-$FePO_4 \cdot H_2O$ templated on E3/E4 virus. Weight loss below 200 °C is from the structural water.

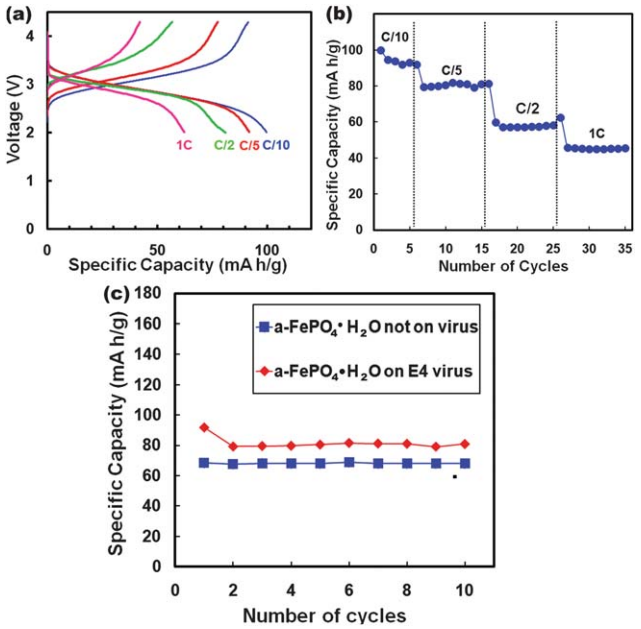

Fig. 5 Electrochemical property of a-$FePO_4 \cdot H_2O$ viral nanowires template on E3/E4 virus tested between 2.0 and 4.3 V. Electrodes were prepared with mass ratio of powder tested : Super P® carbon : PTFE = 80 : 15 : 5. (a) First charge/discharge curves at rates of *C*/10, *C*/5, *C*/2 and 1*C*. (b) Specific discharge capacity upon cycling at different rate : *C*/10, *C*/5, *C*/2 and 1*C*. (c) Specific discharge capacity upon cycling at *C*/5 for ten cycles.

virus coat protein. The particle size of a-$FePO_4 \cdot H_2O$ powder sample synthesized without virus was ~50 nm (Fig. S1†). However, these results are still not satisfactory since the capacity is below 50% of the theoretical value when tested faster than *C*/2 rate. Since a-$FePO_4 \cdot nH_2O$ is electrically insulating, this response is possibly related to the lack of effective electron transport through the composite electrode that suppresses full electrochemical utilization of the active materials. Accordingly, we attempted to increase electronic conductivity of our cathode materials by dispersing conducting additive, silver. For this purpose, we have used two different biological approaches to incorporate silver nanostructures into the a-$FePO_4$ materials.

In the first method "entanglement", separate virus template (also E3/E4) to grow silver nanowires was used and a solution of Ag nanowires grown on E3/E4 virus (Fig. 6(a)) was mixed with a-$FePO_4 \cdot H_2O$ solution for entangled a-$FePO_4 \cdot H_2O$/Ag nanowires network formation (Fig. S2(a)† for TEM image). In the second method "heterostructure", both materials were nucleated on the same wire. Uniformly distributed fine (~5 nm) silver nanoparticles were loaded first along the virus.[7] Amorphous iron phosphate nanowires were produced next on this silver nanoparticles (Ag NPs) loaded E3/E4 virus. When $Fe(NO_3)_3 \cdot 9H_2O$ was used for an iron precursor, silver nanoparticles embedded hydrated amorphous iron phosphates ((Ag)a-$FePO_4 \cdot H_2O$) were synthesized on the virus (Fig. S2(b)† for TEM image). Structural water content was confirmed by TGA as 10.4 wt% (Fig. 6(b)). (Metallic Ag did not show mass change in the temperature range investigated in TGA.) Ag NPs content was 5.1 wt% by DCP-AES. However, when $FeCl_3 \cdot 6H_2O$ was used as an iron precursor, a different material was synthesized. This material has no structural water in TGA (AgCl did not show mass change in the temperature range investigated in TGA and only melted at 455 °C (Fig. S3†)) and shows only silver chloride (AgCl) as crystalline peaks in XRD.[7] From these results, these nanowires were denoted as (AgCl)a-$FePO_4$. Through the comparison with (Ag)a-$FePO_4 \cdot H_2O$ growth using $Fe(NO_3)_3 \cdot 9H_2O$, we speculate that the dehydration of a-$FePO_4 \cdot H_2O$ is associated with the chlorination of Ag NPs, which could occur during the incubation with the $FeCl_3 \cdot 6H_2O$. Assisted by virus templates which could control the structures at the nanoscale, dehydration of structural water without thermal treatment was accomplished by low-temperature and environmentally benign chemistry. The dehydration of structural water increases the theoretical capacity to 178 mA h g^{-1} by decreasing molecular weight, making it a good cathode material.

The electrochemical performance of various viral a-$FePO_4$ nanowires as a lithium ion battery cathode was evaluated and compared (Fig. 7). In Fig. 7, all electrodes were prepared with mixing ratio of power tested : Super P® carbon : PTFE = 80 : 15 : 5 and specific discharge capacities at *C*/5 rate for 10 cycles are presented. With the addition of Ag nanowires, specific capacity increased from 80 mA h g^{-1} (without Ag nanowires) to 90 mA h g^{-1}. However, specific capacity improvement was more pronounced for the heterostructured nanowires. The first discharge capacity of (Ag)a-$FePO_4 \cdot H_2O$ viral nanowires was 120 mA h g^{-1} and the capacity was stabilized to 105 mA h g^{-1}. Although Ag nanowires can provide local networks between a-$FePO_4 \cdot H_2O$ and Ag nanowires in the entanglement method, they cannot make percolating networks since Ag nanowires tend to aggregate by themselves rather than making a well dispersed

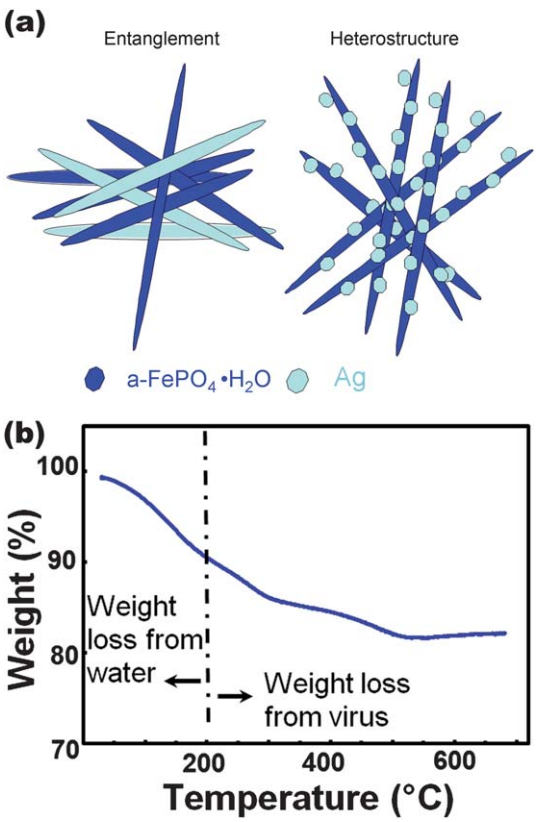

Fig. 6 (a) Schematic presentation of two biological methods: entanglement and heterostructure. (b) TGA curve of the heterostructure, (Ag)a-$FePO_4 \cdot H_2O$ viral nanowires.

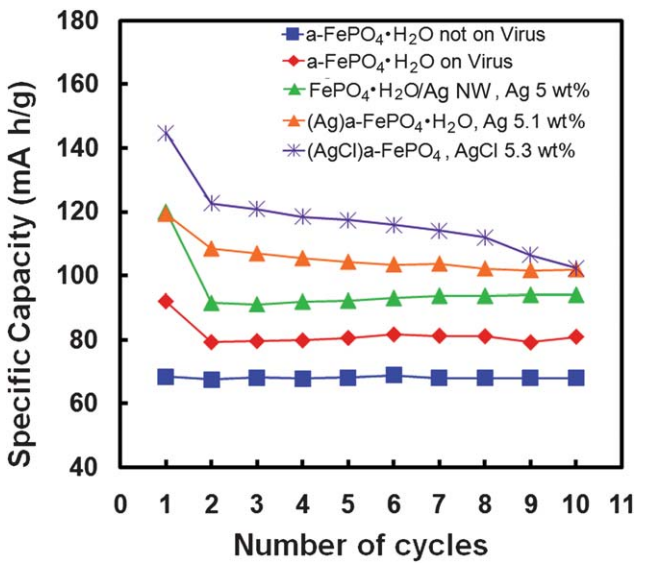

Fig. 7 Comparison of discharge capacities of various nanostructured viral cathodes tested between 2.0 and 4.3 V at *C*/5 rate for ten cycles. Electrodes were prepared with mass ratio of powder tested : Super P® carbon : PTFE = 80 : 15 : 5. Beneficial effects of uniformly distributed conducting nanoparticles and dehydration were clearly shown.

network throughout the whole system. In addition, due to the high gravimetric density of Ag metal (10.5 g cm^{-3}), it is difficult to exceed the percolation threshold volume with the amount of 5 wt% even if it is well dispersed. The beneficial effect of Ag NPs in the heterostructure method over Ag nanowires thus can be considered that efficient interparticle bridge formation between a-$FePO_4 \cdot H_2O$ particles provided by uniformly dispersed Ag NPs throughout the entire system is more advantageous than locally limited network formation by Ag nanowires in enhancing overall electronic conductivity through the whole composite electrode. This argument is supported by impedance analysis (Fig. S4†). The size of semicircles in medium frequency represents bulk resistance while the high frequency semicircles are associated with the particle to particle contacts with size of semicircle reflecting contact resistance.[16,26] The size of medium frequency semicircle systematically decreased from a-$FePO_4 \cdot H_2O$ to a-$FePO_4 \cdot H_2O$/Ag NW and to (Ag)a-$FePO_4 \cdot H_2O$ indicating decreases in bulk resistance. Further capacity improvement was achieved in the heterostructure method with dehydration. The best capacity was obtained with the anhydrous (AgCl)a-$FePO_4$ viral nanowires that have higher theoretical capacity than other nanowires in this study. The heterostructured (AgCl)a-$FePO_4$ viral nanowire electrodes gave the highest first discharge capacity of 145 mA h g^{-1}, however, showed poor capacity retention upon cycling. The capacity decreased to ~100 mA h g^{-1} within 10 cycles. The poor cycling property might be associated with the volume change during the reduction of AgCl (density = 5.56 g cm^{-3}) to metallic Ag (density = 10.5 g cm^{-3}) that occurred during electrochemical test.[7] This irreversible reduction possibly contributed to the first cycle irreversible capacity also. Although reduced metallic Ag could increase local electronic conductivity if the contacts are intact, the volume change could disrupt intimate contacts between particles increasing internal resistance.

To accommodate the volume change and thus improve cycling property, electrodes were prepared with increased carbon content. Increased carbon content could ensure contacts between particles even when there is a moderate volume change during the electrochemical test. In Fig. 8(a), the capacity retention improvement of (AgCl)a-$FePO_4$ viral nanowires is clearly demonstrated as expected. Since the theoretical capacity has been increased due to dehydration, the discharge capacity was higher than that of a-$FePO_4 \cdot H_2O$ nanowires and (Ag)a-$FePO_4 \cdot H_2O$. When we compare the percentage of utilization (experimental/theoretical capacity) of each electrodes at *C*/5 rate second cycle, (AgCl)a-$FePO_4$ and (Ag)a-$FePO_4 \cdot H_2O$ appeared similar as 72 and 71%, respectively, while a-$FePO_4 \cdot H_2O$ showed lower percentage of utilization of 61%. The two heterostructured materials perform similarly in this respect, but the absolute specific capacity value is higher for (AgCl)a-$FePO_4$ with lower molecular mass. Nyquist plot in Fig. 8(b) shows the high-medium frequency impedance response of (AgCl)a-$FePO_4$ viral nanowires before and after the electrochemical test. In most cases, both contact impedance and charge transfer impedance increase with cycling.[26] In Fig. 8(b), (AgCl)a-$FePO_4$ viral nanowires electrodes did not show significant particle to particle contact impedance before test. After 35 cycles of test, high frequency impedance associated with particle to particle contacts increases, however, bulk resistance decreases with cycling for (AgCl)a-$FePO_4$. This unusual behavior could be caused by the reduction of AgCl to metallic Ag with cycling. The reduced metallic Ag enhances electronic conductivity, in other words, decreases bulk resistance in the composite electrodes during cycling.

The rate performance of (AgCl)a-$FePO_4$ viral nanowires as lithium ion battery cathodes was evaluated with a signature curve

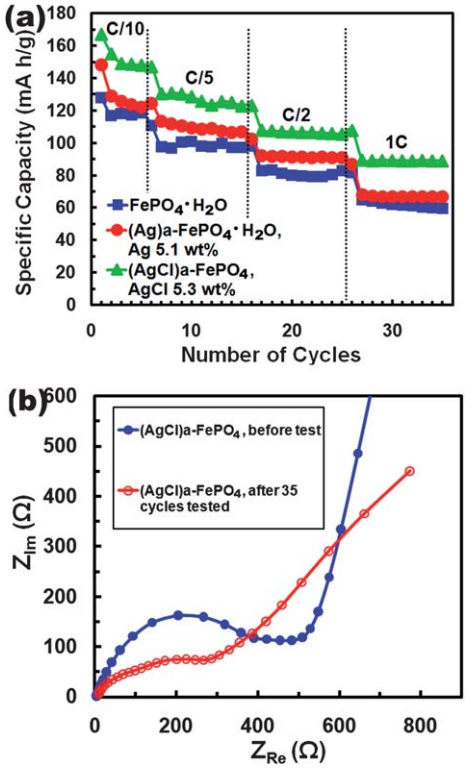

Fig. 8 Electrochemical performance of heterostructured viral nanowires on E3/E4 tested between 2.0 and 4.3 V. Electrodes were prepared with mass ratio of powder tested : Super P® carbon : PTFE = 70 : 25 : 5. (a) Comparison of specific discharge capacity upon cycling at different rate: *C*/10, *C*/5, *C*/2 and 1*C*. (b) Nyquist plot: impedance responses of (AgCl)a-$FePO_4$ viral nanowires before and after electrochemical test.

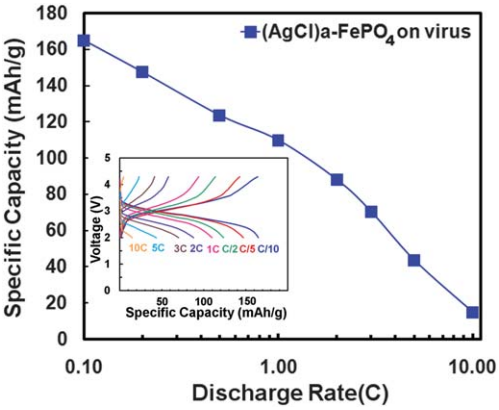

Fig. 9 Rate performance of (AgCl)a-$FePO_4$ viral nanowires. Evolution of specific discharge capacities as a function of test rate. Inset: first charge/discharge curves of (AgCl)a-$FePO_4$ viral nanowires on E3/E4 tested between 2.0 and 4.3 V at different rates. Electrodes were prepared with mass ratio of powder tested : Super P® carbon : PTFE = 70 : 25 : 5.

and first charge/discharge curves at various rates (Fig. 9). The first discharge capacity at a low discharge rate of *C*/10 was 165 mA h g^{-1} (93% of the theoretical value) and that of 1*C* discharge rate was 110 mA h g^{-1}. These rate performance values are slightly inferior but comparable to the best reported values for a-$FePO_4$ synthesized at high temperature.[16] The designing of structure at the nanoscale for advanced electrodes was facilitated even with this simple virus system with only one gene modified for negative surface charges, enabling an enhanced performance by an efficient low temperature process.

Conclusion

Synthesis and nanostructure design of amorphous iron phosphate (a-$FePO_4 \cdot nH_2O$, $n = 0$ or 1) in size regime of a few tens of nm have been realized by using genetically engineered M13 virus template for 3 V lithium ion battery cathodes. The negatively charged E3/E4 virus served as a powerful template for the nanosized a-$FePO_4$ growth in this study by forming conjugates with Fe^{3+} ions preventing hydrolysis of these ions. The versatile E3/E4 virus accomplished uniform distribution of silver through the whole system by heterostructure formation along the single virus scaffold enhancing battery performances. The biological template and synthetic chemistry were synergistically combined in producing anhydrous a-$FePO_4$ without thermal treatment *via* low-temperature and eco-efficient chemistry increasing the specific capacity of the materials tested. The electrochemical properties reported in this work are comparable to the best reported values for a-$FePO_4$ synthesized at high temperature. We anticipate that further use of biological principles and scaffolds will give additional versatility and flexibility in the advanced nanomaterial design for next generation green energy systems.

Acknowledgements

This work was supported by the Army Research Office Institute of the Institute of Collaborative Biotechnologies (ICB) and US National Science Foundation through the Materials Research Science and Engineering Centers program.

References

1 J. M. Tarascon, *Nat. Nanotechnol.*, 2009, **4**, 341.
2 J. M. Tarascon, C. Delacourt, A. S. Prakash, M. Morcrette, M. S. Hegde, C. Wurm and C. Masquelier, *Dalton Trans.*, 2004, 2988.
3 F. Croce, A. D. Epifanio, J. Hassoun, A. Deptula, T. Olczac and B. Scrosati, *Electrochem. Solid-State Lett.*, 2002, **5**, A47.
4 Y. S. Hu, Y. G. Guo, R. Dominko, M. Gaberscek, J. Jamnik and J. Maier, *Adv. Mater.*, 2007, **19**, 1963.
5 A. S. Arico, P. Bruce, B. Scrosati, J. M. Tarascon and W. Van Schalkwijk, *Nat. Mater.*, 2005, **4**, 366.
6 L. Taberna, S. Mitra, P. Poizot, P. Simon and J. M. Tarascon, *Nat. Mater.*, 2006, **5**, 567.
7 Y. J. Lee, H. Yi, W. J. Kim, K. Kang, D. S. Yun, M. S. Strano, G. Ceder and A. M. Belcher, *Science*, 2009, **324**, 1051.
8 Y. G. Wang, Y. R. Wang, E. J. Hosono, K. X. Wang and H. S. Zhou, *Angew. Chem., Int. Ed.*, 2008, **47**, 7461.
9 B. Kang and G. Ceder, *Nature*, 2009, **458**, 190.
10 S. Y. Chung, J. T. Bloking and Y. M. Chiang, *Nat. Mater.*, 2002, **1**, 123.
11 C. Delacourt, P. Poizot, S. Levasseur and C. Masquelier, *Electrochem. Solid-State Lett.*, 2006, **9**, A352.
12 P. P. Prosini, M. Lisi, S. Scaccia, M. Carewska, F. Cardellini and M. Pasquali, *J. Electrochem. Soc.*, 2002, **149**, A297.
13 Y. N. Song, S. F. Yang, P. Y. Zavalij and M. S. Whittingham, *Mater. Res. Bull.*, 2002, **37**, 1249.
14 F. Croce, A. D'Epifanio, P. Reale, L. Settimi and B. Scrosati, *J. Electrochem. Soc.*, 2003, **150**, A576.
15 Z. C. Shi, Y. X. Li, W. L. Ye and Y. Yang, *Electrochem. Solid-State Lett.*, 2005, **8**, A396.
16 Z. C. Shi, A. Attia, W. L. Ye, Q. Wang, Y. X. Li and Y. Yang, *Electrochim. Acta*, 2008, **53**, 2665.
17 B. K. Kay, J. Winter and J. McCafferty, *Phage Display of Peptides and Proteins: a Laboratory Manual*, 1996.
18 D. N. Krag, G. S. Shukla, G. P. Shen, S. Pero, T. Ashikaga, S. Fuller, D. L. Weaver, S. Burdette-Radoux and C. Thomas, *Cancer Res.*, 2006, **66**, 7724.
19 S. R. Whaley, D. S. English, E. L. Hu, P. F. Barbara and A. M. Belcher, *Nature*, 2000, **405**, 665.
20 Y. Huang, C. Y. Chiang, S. K. Lee, Y. Gao, E. L. Hu, J. De Yoreo and A. M. Belcher, *Nano Lett.*, 2005, **5**, 1429.
21 K. T. Nam, D. W. Kim, P. J. Yoo, C. Y. Chiang, N. Meethong, P. T. Hammond, Y. M. Chiang and A. M. Belcher, *Science*, 2006, **312**, 885.
22 K. T. Nam, R. Wartena, P. J. Yoo, F. W. Liau, Y. J. Lee, Y. M. Chiang, P. T. Hammond and A. M. Belcher, *Proc. Natl. Acad. Sci. U. S. A.*, 2008, **105**, 17227.
23 K. T. Nam, Y. J. Lee, E. M. Krauland, S. T. Kottmann and A. M. Belcher, *ACS Nano*, 2008, **2**, 1480.
24 R. T. Clay and R. E. Cohen, *Supramol. Sci.*, 1998, **5**, 41.
25 Y. S. Hong, K. S. Ryu, Y. J. Park, M. G. Kim, J. M. Lee and S. H. Chang, *J. Mater. Chem.*, 2002, **12**, 1870.
26 K. Sheem, Y. H. Lee and H. S. Lim, *J. Power Sources*, 2006, **158**, 1425.